Helsinki University of Technology Radio Laboratory Publications
Teknillisen korkeakoulun Radiolaboratorion julkaisuja
Espoo, March, 2002 REPORT S 252

DESIGN AND BANDWIDTH OPTIMIZATION OF DUAL-RESONANT PATCH ANTENNAS

Jani Ollikainen Pertti Vainikainen

TEKNILLINEN KORKEAKOULU
TEKNISKA HÖGSKOLAN
HELSINKI UNIVERSITY OF TECHNOLOGY
TECHNISCHE UNIVERSITÄT HELSINKI
UNIVERSITE DE TECHNOLOGIE D'HELSINKI

Distribution:
Helsinki University of Technology
Radio Laboratory
P.O.Box 3000
FIN-02015 HUT
Tel. +358-9-451 2252
Fax. +358-9-451 2152

ISBN 951-22- 5891-9
ISSN 1456-3835

Otamedia Oy
Espoo 2002

Abstract

One of the most effective methods of increasing the impedance bandwidth of narrow-band resonant antennas, such as microstrip patches, is adding one or more resonators into an antenna structure in order to make it dual-resonant or multiresonant. In this paper, the most important electrical design parameters concerning the bandwidth optimization of dual-resonant patch antennas are systematically analyzed with a lumped-element circuit model. Furthermore, it is shown how the impedance bandwidth of a given antenna structure can be optimized by adjusting these parameters. Based on the circuit model, novel simple equations that enable the prediction of optimal dual-resonant impedance bandwidth are also derived. To support the theory, examples with various antenna structures are presented. In a parameter study for a stacked shorted patch antenna, it is shown that the electrical parameters of the circuit model have real world counterparts as dimensions of a real antenna. It is also shown with the circuit model and with a real antenna structure that by exciting two optimally coupled resonant modes with equal unloaded quality factors, the impedance bandwidth of a square-shaped open-circuited microstrip patch antenna can be increased by as much as a factor of 3.4 without increasing its size. As the last example, three different dual-resonant shorted patch antenna realizations are compared with the circuit model and with a full-wave electromagnetic simulator. The comparison reveals the existence of a non-radiating resonant mode, which can reduce the bandwidth improvement obtained with the studied dual-resonant antenna structures.

Contents

1 Introduction

Microstrip patch antennas are resonant antennas with many favorable characteristics, such as low cost, light weight, and low profile. Their main limitation is narrow impedance bandwidth, which is known to be approximately proportional to the volume of the antenna measured in wavelengths [1], [2]. Thus, the impedance bandwidth of a basic patch antenna can be optimized by selecting a low-permittivity substrate, which maximizes the resonant length of the patch, and by maximizing the patch width and substrate thickness (antenna height). However, in many applications, such as inside portable radio devices, the space allowed for the antenna is limited, which restricts the antenna size. Furthermore, the size may be limited by feeding technique, radiation pattern and efficiency related constraints [3].

Besides increasing the size, the bandwidth of a microstrip patch antenna can be increased by artificially decreasing its efficiency. In many cases, this is, however, unacceptable. Although, as pointed out in [4], the manufacturing simplicity of this technique has a definite appeal. In some applications, it can outweigh the disadvantage of decreased gain.

When the size and efficiency are fixed, the bandwidth of a patch antenna can be increased significantly only by adding one or more resonators into the antenna structure. Depending on the number of added resonators, this leads to dual-resonant or multiresonant antenna structures. Typically one resonator is added, which can be realized by adding a lossless matching resonator [5]–[11], a stacked parasitic patch [12]–[17] or a coplanar parasitic patch [18]–[23]. A resonant slot has also been used [24], and in principle, any resonant structure can be used. Adding resonators to an antenna structure will usually increase the design complexity and may also increase the manufacturing costs.

Previously, the design of various dual-resonant patch antenna structures with increased bandwidth has been discussed in several papers. The design of aperture-coupled and probe-fed open-circuited stacked patches has been treated in [13] and [25], respectively. The effects of several geometrical design parameters on the input impedance of a stacked short-circuited patch antenna have been discussed first in [17] and more thoroughly in [26]. The design of open-circuited patches with coplanar parasitics has been presented in [27]. The effects of various geometrical design parameters on the input impedance of a shorted patch with a coplanar parasitic have been studied in [22] and [28]. Despite the differences in antenna

configurations, the main electrical design parameters can be noticed to have the same effect on the impedance behavior of all the dual-resonant antennas presented in the above-mentioned papers. Therefore, it is clear that they all can be designed following the same basic principles. Although, perhaps noticed by some designers in the antenna industry, to the authors' knowledge this general conclusion has not been drawn and presented in the open literature. The basic design principles of dual-resonant antennas can be presented using an equivalent circuit model, which can be used as the basis for a simple theory that facilitates the design and gives insight into the operation and characteristics of various dual-resonant antenna structures.

Dual-resonant antennas have the characteristic feature of a doubly looped impedance locus on the Smith chart. It is shown in [13], [22], [25]–[27] how the impedance bandwidth can be increased by moving the small loop (coupling loop) in the impedance locus to the center of the Smith chart. It is also mentioned in [13], [22], [26], [27] that the impedance bandwidth depends on the size of the coupling loop. However, to the author's knowledge, so far a connection between the optimal impedance bandwidth, optimal shape of the impedance locus, and optimal size of the coupling loop has not been systematically established. Furthermore, it has not been clear which characteristics affect the optimal shape of the locus, or how critical they are from the bandwidth point of view.

The impedance bandwidth of small resonant antennas is known to depend on the antenna size [29], [30]. Therefore, any extra bandwidth, obtained by optimizing the antenna performance, can be traded off for smaller size. The constant requirements to decrease the antenna size and to increase the number of antenna elements that can be fitted into a given volume make bandwidth optimization especially important in the case of internal mobile phone antennas, which is currently one of the main application areas of microstrip type small antennas. Irrespective of the application, decreased antenna size obtained through bandwidth optimization is favorable as it reduces the material costs and weight of the antennas.

The purpose of this paper is to present a unified theory for the optimization of impedance bandwidth of dual-resonant patch antennas. The theory is based on a simple lumped-element circuit model, which can be used in the presented form at least for both open-circuited and short-circuited stacked patches, patches with a coplanar parasitic patch, and patches with one lossless matching resonator. The purpose of the circuit model is to provide information that helps reducing the number of iterations required to optimize the bandwidth of a given dual-resonant antenna structure either experimentally or with a full-wave electromagnetic

simulator. In the paper, the circuit model is used to systematically identify and analyze the most important electrical design parameters concerning the bandwidth optimization of dual-resonant patches. It is also shown on the Smith chart, which is a very useful tool in the design, how the main design parameters affect the input impedance of the antenna, and how these parameters can be used in the design and optimization. Furthermore, it is shown that the impedance locus of a bandwidth-optimized dual-resonant patch has a certain shape on the Smith chart, and therefore a quick look at the impedance result will tell the designer how well the antenna is optimized. Based on the circuit model, novel equations enabling e.g. literature-based bandwidth predictions are derived and presented. It will also be shown in the paper that the electrical parameters of the model have real world counterparts as dimensions of a real antenna. This verifies the model and also shows some of its limitations. The use of the circuit-model also reveals a potential problem of dual-resonant and multiresonant antennas, which to the authors' knowledge has not been discussed to this extent previously in open literature. Microstrip patch antennas are used as examples of resonant antennas throughout the paper. It is, however, clear that the presented main principles apply to all dual-resonant antennas that can be adequately modeled with simple resonant circuits.

2 Circuit Model for Dual-Resonant Patch Antennas

2.1 Description of Model

As an example of dual-resonant patch antennas, the stacked shorted patch antenna is shown in Fig. 1a. It consists of a driven lower patch, a parasitically coupled upper patch, and two short-circuiting elements. One of the short-circuiting elements connects the lower patch to the ground plane; the other one connects the upper patch to the shorted end of the lower patch or directly to the ground plane. In this case, the antenna is fed by a probe. Other feeding methods are of course also possible. In Fig. 1a, the heights h_1 and h_2 are measured from the upper surface of the ground plane to the lower surface of the corresponding patch. The patch lengths l_1 and l_2 are measured from the inner surface of the shorting plate to the open end of the corresponding patch.

Near the resonant frequency, the impedance characteristics of an open-circuited or a short-circuited patch antenna (or planar inverted-F antenna / PIFA) can be modeled as a parallel resonant circuit [31], [32]. The single resonator model can be extended to dual-resonant antennas by adding to it another resonant circuit, which represents the parasitic patch. Based on the impedance behavior on the Smith chart, this can be done by adding a series resonant circuit which is coupled to the driven resonator by an ideal transformer as shown in Fig. 1b [26], [33]. In the model of Fig. 1b, the resonators have to be of different type in order to describe a dual resonance. Otherwise, the circuit can be easily simplified into a single-resonant circuit. A model equivalent to that of Fig. 1b can be obtained by replacing the second ideal transformer and the series resonant circuit in Fig. 1b by an admittance inverter and parallel resonant circuit. The admittance inverter can be further approximated e.g. by a series capacitor as in [34], [35]. Another equivalent alternative to the model of Fig. 1b can be obtained with two impedance inverters and two series resonators [36]. Lumped-element circuit models for various dual-resonant patch antennas have also been presented in [2], [8], [10], [11], [34], [35]. The model used in [8], [10], [11] is only intended for the design of a non-radiating matching circuit. The model of Fig. 1b is here preferred to those of [2], [34], [35] because it allows the derivation of simple equations for the optimal bandwidths of dual-resonant antennas, which is one of the main results of this paper. The model of Fig. 1b is also more general than those of [2], [34], [35] and enables a demonstration of all the main parameters needed in the bandwidth optimization.

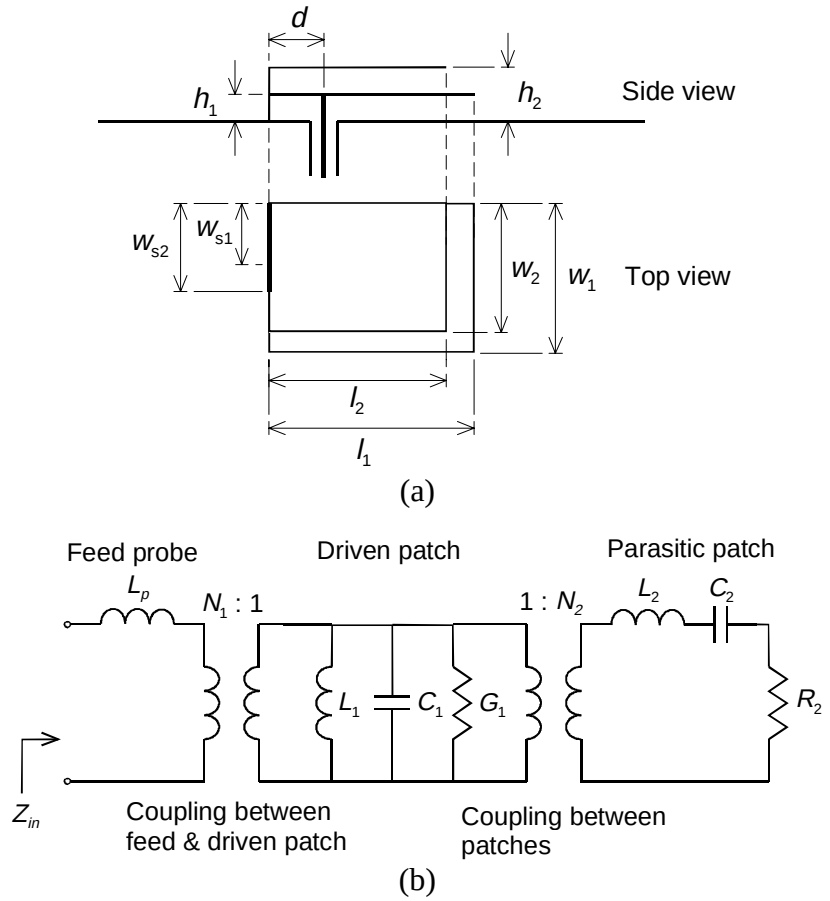

Figure 1. *a) Geometry of a stacked shorted patch antenna. b) Circuit model for a dual-resonant patch antenna.*

The input impedance of the circuit of Fig. 1b can be written

$$Z_{in} = \mathrm{j}\omega L_p + \frac{k_1}{\dfrac{1}{\mathrm{j}\omega L_1} + \mathrm{j}\omega C_1 + G_1 + \dfrac{k_2}{\mathrm{j}\omega L_2 + \dfrac{1}{\mathrm{j}\omega C_2} + R_2}}, \tag{1}$$

where $k_1 = N_1^2$ and $k_2 = N_2^2$. The first ideal transformer in the model represents the coupling of the feed to the driven patch. The value of the coupling coefficient k_1 increases as the coupling gets stronger. For example, in Fig. 1a this is equivalent to moving the feed probe away from the short circuit and towards the open end of the patch (*d* increases). The second transformer represents the coupling between the driven and the parasitic patch. The value of k_2 increases, as the coupling gets stronger. For example, the coupling between the patches of a stacked shorted patch antenna can be adjusted by varying the distance between the open ends of the patches as will be shown later in the text. The component values of the parallel and series resonant circuit in Fig. 1b and in Eq. (1) are related to the unloaded quality factors of the resonators as given by Eqs. (2) and (3), respectively [37].

$$Q_{01} = \frac{\omega_{r1} C_1}{G_1} = \frac{1}{G_1 \omega_{r1} L_1} \tag{2}$$

$$Q_{02} = \frac{\omega_{r2} L_2}{R_2} = \frac{1}{R_2 \omega_{r2} C_2} \tag{3}$$

In Eqs. (2) and (3), ω_{r1} and ω_{r2} are the angular resonant frequencies of the driven (lower) and parasitic (upper) patch, respectively (see Fig. 1a). The unloaded quality factors of the lower and the upper patch are denoted by Q_{01} and Q_{02}, respectively. The main parameters that are used to study the behavior of the model are f_{r1}, f_{r2}, k_1, k_2, Q_{01}, and Q_{02}. When the input impedance of a probe-fed patch antenna is modeled, the series inductance of the probe L_p can be used as the first component in the circuit. To provide a more general presentation and to show the effects of the main parameters more clearly, L_p is removed from the circuit at this point ($L_p = 0$). However, its effect will be discussed later in the text. For the calculations, the inductances of L_1 and L_2 have been normalized to $L_1 = L_2 = 1/2\pi$. This affects the values of k_1 and k_2, which are required for a certain response. Furthermore, the center frequency of the model has been normalized to $f_c = 1$ and the reference impedance level to $Z_0 = 1$.

2.2 BANDWIDTH ENHANCEMENT FACTOR

The increase of bandwidth obtained with a dual-resonant antenna can be described using the bandwidth enhancement factor F calculated from

$$F = \frac{B_{dr}}{B_{sr,opt}}, \tag{4}$$

where B_{dr} is the bandwidth of the studied dual-resonant antenna, and $B_{sr,opt}$ is the bandwidth of an optimized single-resonant reference antenna. $B_{sr,opt}$ can be calculated from

$$B_{sr,opt} = \frac{S^2 - 1}{2SQ_0}, \tag{5}$$

where S is the maximum allowed voltage standing wave ratio (*VSWR*), and Q_0 is the unloaded quality factor of the antenna. Eq. (5) can be obtained from Eqs. (6) and (8) of [7] (or by simplifying Eq. (21) of [38]). Because the bandwidth of a patch antenna depends on its size in wavelengths, the single-resonant and dual-resonant antennas should be equal in size to obtain a fair comparison.

Figure 2 shows examples of bandwidth enhancement factors (F) as a function of the ratio of the resonant frequencies of the resonators (f_{r2}/f_{r1}) when $L_p = 0$. The values of B_{dr} needed for

the calculation of the curves of Fig. 2 have been obtained with the model of Fig. 1b ($L_p = 0$) by testing all relevant value combinations of k_1 and k_2 at each value of f_{r2}/f_{r1}. The unloaded quality factors used in the calculations are $Q_0 = 14.9$ and $Q_{01} = Q_{02} = 23.9$. The first one is for a single-resonant reference antenna. The last two are for a shorted patch with a coplanar parasitic. They were obtained in [33] by dividing the reference antenna into two narrower equally sized patches. The quality factors were approximated from [32] (p. 174, Fig. 5.9) for 5 mm-thick ($0.03\lambda_0$) shorted patches with the width-to-length ratios $w/l = 1$ ($Q_0 = 14.9$) and $w/l = 0.5$ ($Q_{01} = Q_{02} = 23.9$). It is assumed in the calculations that the Q_0 of an isolated patch antenna can be used to approximate that of the same patch with another patch positioned in its proximity. For a stacked shorted patch, Q_{01} and Q_{02} are not likely to be equal, but using more appropriate values, such as $Q_{01} = 28.7$ and $Q_{02} = 9.3$, would cause only minor changes in the main results of Figs. 2 to 6. Therefore, the selected values $Q_0 = 14.9$ and $Q_{01} = Q_{02} = 23.9$ can be used to illustrate the basic behavior of the model for both coplanar and stacked dual-resonant patches. In some calculated cases, two separate bands were obtained. In those cases, the band with the larger relative bandwidth was selected. Fig. 2 shows that in the case $L_p = 0$, the maximum bandwidth enhancement factor (F_{max}) for the circuit of Fig. 1b is obtained when $f_{r1} = f_{r2}$. According to simulations, when $L_p = 0$, the frequency ratio at which F reaches its maximum does not depend on the Q_0s of the resonators or the used matching requirement.

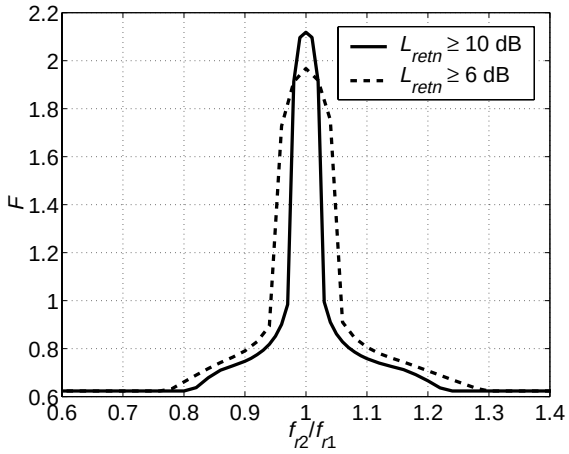

Figure 2. *Bandwidth enhancement factor (F) as a function of resonant frequency ratio (f_{r2}/f_{r1}) for matching requirements $L_{retn} \geq 10$ dB and $L_{retn} \geq 6$ dB ($Q_0 = 14.9$, $Q_{01} = Q_{02} = 23.9$).*

2.3 Optimal Shape of Impedance Locus

The optimal shape of the impedance locus (on the Smith chart), which gives the maximum bandwidth, can be determined by selecting the coupling coefficients k_1 and k_2 that in Fig. 2 give the largest bandwidth enhancement factor and by plotting the reflection coefficient as a

function of frequency. Figure 3a shows the optimized reflection coefficients when the matching requirements are $L_{retn} \geq 10$ dB (solid line) and $L_{retn} \geq 6$ dB (dashed line). The optimal coupling coefficients for $L_{retn} \geq 10$ dB are $k_{1,opt} = 1.317 \times 10^{-1}$ and $k_{2,opt} = 8.855 \times 10^{-3}$. For $L_{retn} \geq 6$ dB, they are $k_{1,opt} = 1.958 \times 10^{-1}$ and $k_{2,opt} = 2.291 \times 10^{-2}$. As shown in Fig. 3a, the maximum bandwidth is obtained when the small loop in the impedance locus (*coupling loop*) is just slightly smaller than the largest loop that would fit inside the circle representing the minimum allowed return loss (e.g. $L_{retn} \geq 10$ dB, dashed circle). The shapes of the optimal impedance loci for matching requirements $L_{retn} \geq 10$ dB and $L_{retn} \geq 6$ dB are almost identical, their sizes have only been scaled according to the minimum allowed L_{retn}. The optimal size of the coupling loop depends on the ratio Q_{01}/Q_{02}, as shown is Fig. 3b. The size of the loop is the smallest when Q_{01}/Q_{02} is the smallest and the largest when Q_{01}/Q_{02} is the largest. The values of Q_{01} and Q_{02} have no effect on the optimal shape of the locus as long as their ratio is constant. When the values of Q_{01} and Q_{02} change, the optimal impedance bandwidth changes, and the frequency points slide along the optimally shaped locus. Regardless of the ratio Q_{01}/Q_{02}, when $L_p = 0$, the optimal input impedance at the center frequency is always Z_0/S for the circuit of Fig. 1b. As shown in Fig. 3b, when $Q_{01} = \infty$, the input impedance at the upper and lower bound of the impedance band is Z_0S.

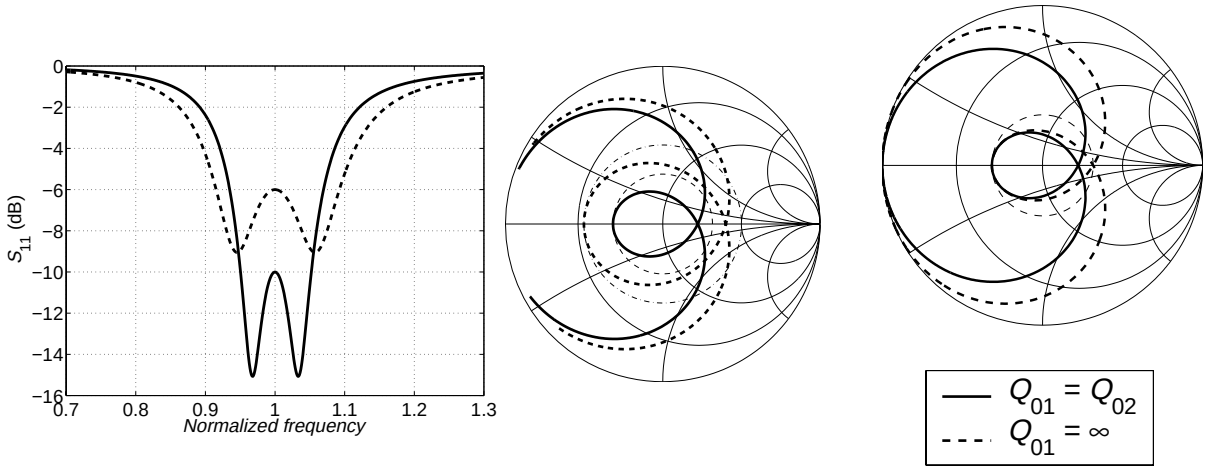

(a) (b)

Figure 3. *a) Optimized frequency responses of reflection coefficient and optimized input impedance loci for the dual-resonant circuit of Fig. 1b when matching requirements are $L_{retn} \geq 10$ dB (solid) and $L_{retn} \geq 6$ dB (dashed), ($Q_{01} = Q_{02} = 23.9$ and $f_{r1} = f_{r2} = f_c = 1$). Dashed circle on the Smith chart represents $L_{retn} = 10$ dB and dashdot circle $L_{retn} = 6$ dB. b) Optimized input impedance loci for the dual-resonant circuit of Fig. 1b when $Q_{01} = Q_{02}$ and when the first resonator is lossless ($Q_{01} = \infty$). Dashed circle on the Smith chart represents $L_{retn} = 10$ dB.*

The impedance bandwidth of a dual-resonant antenna with given Q_{01} and Q_{02} depends on the size and position of the coupling loop relative to the circle representing minimum allowed return loss. This can be seen in Fig. 4a which shows examples of frequency responses of reflection coefficient for an optimal case with $F \approx 2.2$ (thick solid line), two nearly optimal cases with $F \approx 2.0$ (thick dashed and dashdot line), and two poorly optimized cases (thin solid and dashed line). Figure 4a also shows that the size of the coupling loop on the Smith chart can vary considerably without a major reduction of bandwidth from the optimum value as long as the coupling of the feed to the driven resonator (k_1) is adjusted so that the small loop touches the circle representing the minimum allowed return loss at the center frequency (in Fig. 4a, $Z_{in}(f = f_c) = Z_0/S$). If k_1 is too small or too large, the bandwidth will be substantially reduced. When k_1 is too large, as in Fig. 4a (thin solid line), the behavior of a dual-resonant antenna structure can be easily confused with that of a single-resonant antenna, if only the magnitude of the reflection coefficient is studied. As shown already in Fig. 3b, the optimal size of the coupling loop depends somewhat on the ratio Q_{01}/Q_{02}. Generally, however, good or nearly optimal results are obtained in typical cases ($Q_{01} \geq Q_{02}$) always when the size of the coupling loop is approximately equal or preferably just slightly smaller than the size of the return loss circle.

A more general perspective on optimizing a dual-resonant impedance response can be obtained by plotting the bandwidth enhancement factor (F) as a function of the coupling coefficients k_1 and k_2, as in Fig. 4b. It confirms that significant increase of bandwidth ($F \geq 2$) can be obtained over a fairly broad range of k_2 values as long as the coupling between the feed and the driven patch (k_1) is adjusted accordingly. This can also be seen in Fig. 4c, which shows the bandwidth enhancement factor as a function of k_2 for optimal values of k_1. According to Fig. 4b, too strong coupling between the feed and the driven resonator (too large k_1) and too weak coupling between the resonators (too small k_2) are less critical from the optimal bandwidth point of view than the opposite cases. Plots like the ones in Figs. 4b and 4c can be obtained using Eqs. (A11) and (A14) presented in Appendix A.

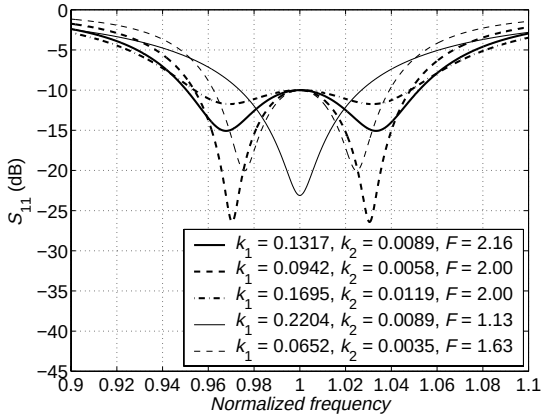

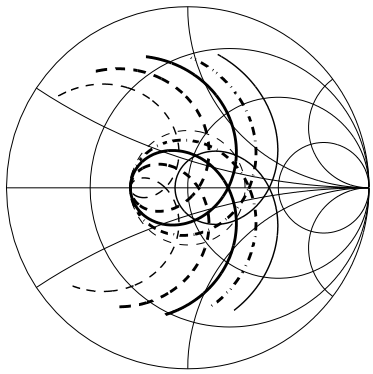

(a)

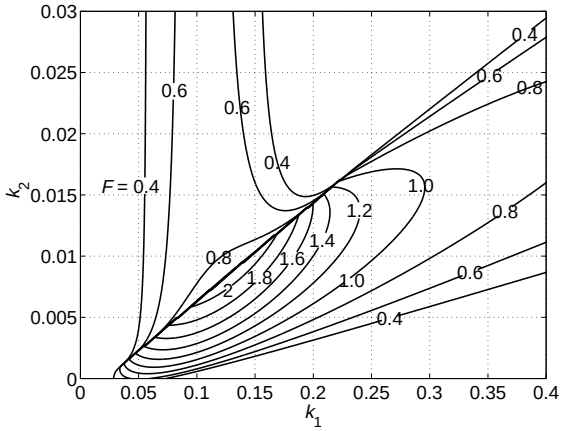

(b)

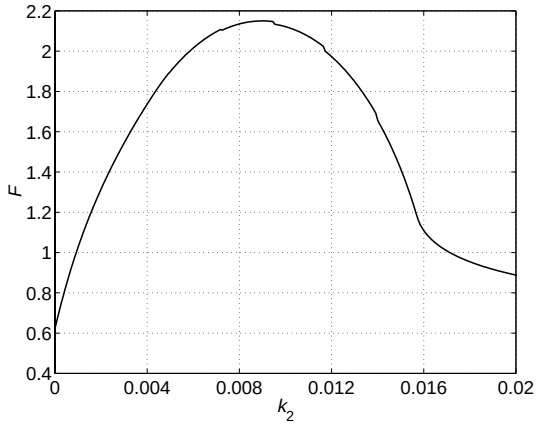

(c)

Figure 4. *a) Optimal ($F \approx 2.2$), nearly optimal ($F \approx 2.0$), and poorly optimized ($F \approx 1.0$ and $F \approx 1.6$) frequency responses of reflection coefficient for the model of Fig. 1b. b) Bandwidth enhancement factor (F) as a function of coupling coefficients k_1 and k_2. c) F as a function of k_2 when k_1 has been optimized (In all graphs $Q_0 = 14.9$, $Q_{01} = Q_{02} = 23.9$, $f_{r1} = f_{r2} = 1$, and $L_p = 0$).*

2.4 Optimization of Impedance Locus on Smith Chart

Next, it will be shown how the impedance locus of a dual-resonant antenna with given Q_{01} and Q_{02} can be optimized by adjusting the resonant frequencies of the driven and parasitic resonator (f_{r2} and f_{r1}) and the coupling coefficients k_1 and k_2. This part is based on a previous paper by the authors [26]. Similar, supporting results have later been presented also in [35].

2.4.1 Resonant Frequencies of Resonators

Figure 5a shows how changing the resonant frequency of the parasitic resonator (f_{r2}) from $0.9f_{r1}$ to $1.1f_{r1}$ affects the size and the position of the coupling loop on the Smith chart. The coupling coefficients k_1 and k_2 have optimal values. When $f_{r2} = f_{r1}$, the impedance locus is

symmetrical relative to the real axis of the Smith chart, and the coupling loop has an optimal size and position inside the circle representing minimum acceptable return loss (thick solid line). The loop shifts towards the low frequency end of the impedance locus when $f_{r2} < f_{r1}$ and towards the high frequency end of the impedance locus when $f_{r2} > f_{r1}$ (f increases clockwise along the impedance locus). In both cases, the shift is the larger, the larger the difference of the resonant frequencies is. Furthermore, the size of the coupling loop decreases as it moves away from the optimal position. Thus, we may conclude that the position of the coupling loop can be optimized by adjusting the relative resonant frequencies of the parasitic and the driven resonator f_{r2}/f_{r1}.

2.4.2 Coupling Between Feed and Driven Resonator

Figure 5b shows how varying the coupling between the feed and the driven resonator (k_1) affects a dual-resonant impedance locus. As in the case of a single resonator, the size of the large loop of the impedance locus increases with coupling making it possible to adjust the position of the coupling loop. When the coupling loop is in optimal position (thick solid line), the feed is overcoupled to the driven resonator. In addition, it seems that the size of the coupling loop reaches its maximum, when the feed is optimally coupled to the driven resonator. As shown in Figs. 5a and 5b, f_{r2}/f_{r1} and k_1 are the only parameters needed to move the coupling loop to the optimal position inside a given return loss circle on the Smith chart.

2.4.3 Coupling Between Resonators

Figure 5c shows the effect of varying the coupling between the driven and parasitic resonator (k_2). The additional small loop on the Smith chart, which is a characteristic feature of dual-resonance, is called the *coupling loop* because its size is proportional to the coupling between the driven and parasitic resonator. The size of the coupling loop is the larger, the stronger the coupling between the resonators is. Optimization of the coupling loop size is important because the impedance bandwidth depends on it, as presented in Sec. 2.3.

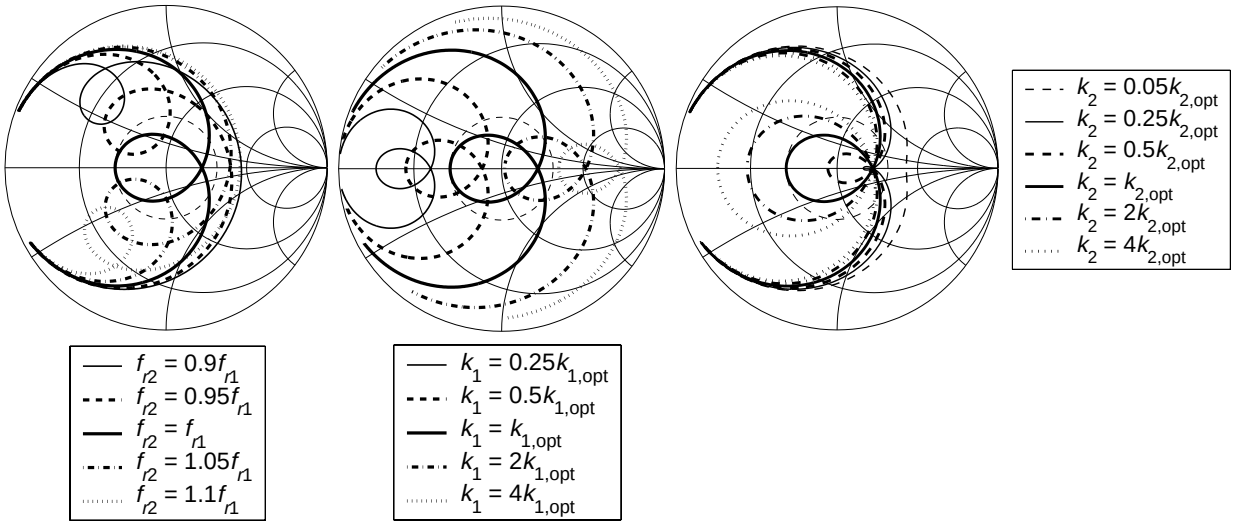

(a) (b) (c)

Figure 5. *Effects of the main design parameters on the input impedance locus of the dual-resonant circuit of Fig. 1b ($Q_{01} = Q_{02} = 23.9$). a) Effect of resonant frequency ratio (f_{r2}/f_{r1}) ($k_1 = k_{1,opt} = 1.317 \times 10^{-1}$ and $k_2 = k_{2,opt} = 8.855 \times 10^{-3}$). b) Effect of coupling between feed and driven resonator ($f_{r1} = f_{r2}$ and $k_2 = k_{2,opt}$). c) Effect of coupling between resonators ($f_{r1} = f_{r2}$ and $k_1 = k_{1,opt}$).*

2.4.4 Summary

Concerning the optimization of the impedance bandwidth, the most important electrical parameters of a dual-resonant patch antenna are the Q_0s and the relative resonant frequencies of the resonators, the coupling between the feed and the driven resonator, and the coupling between the resonators. The Q_0s are important because they define the bandwidth potential of the antenna. The design approach used in this work is based on positioning an optimally sized coupling loop on the Smith chart inside the circle that represents the minimum allowed L_{retn} (see e.g. Fig. 3a). Fig. 5 shows the importance of the other mentioned parameters (f_{r1}/f_{r2}, k_1, and k_2): they are the only ones needed to move the coupling loop from any point on the Smith chart to its center and to optimize the size of the loop for any matching requirement. In practice, the first task in the design process is to identify the primary geometrical parameters of a given antenna structure that control the mentioned electrical parameters. After that, the design and optimization are fairly straightforward following the principles presented in this section. There may of course be practical limitations in the design of various dual-resonant antenna configurations. For example, it may not be possible to implement the necessary coupling coefficients in all cases, such as for very thick probe-fed stacked patches.

2.5 FEED REACTANCE

The series inductance of the probe L_p is typically included in a lumped-element circuit model of a probe-fed patch to improve its accuracy in describing the input impedance, although there are also models where it has been neglected [34], [35]. In the beginning of this paper, L_p was removed from the model of Fig. 1b to show the effects of the main parameters (f_{r2}/f_{r1}, k_1, and k_2) more clearly. The effect of L_p on the maximum bandwidth of a dual-resonant antenna can be seen in Fig. 6a, which shows the bandwidth enhancement factor as a function of the resonant frequency ratio of the resonators for seven different normalized series reactances (x = –3, –2, –1, 0, 1, 2, and 3 at f = 1). The effect of L_p on the maximum bandwidth enhancement factor (F_{max}) seems to be fairly small (< 10 %) for typical inductance values, such as 1…12 nH (which correspond to normalized series reactances of 0.2…2.7 at 1.8 GHz). When the input reactance is 0, F_{max} is obtained when $f_{r1} = f_{r2}$. With an inductive input reactance ($x > 0$), F_{max} is obtained when $f_{r2} > f_{r1}$. It is also possible to feed a patch antenna capacitively. With a capacitive input reactance ($x < 0$), F_{max} is obtained when $f_{r2} < f_{r1}$. In Fig. 6a, the relative widths of the curves obtained with inductive and capacitive reactances are equal (e.g. at the level F = 1.6). For all the values of F in Fig. 6a, the center frequency of the circuit model $f_c \approx 1$.

Figure 6b shows the effects of five normalized series reactances (x = –3, –1, 0, 1, and 3 at $f = f_c = 1$) on the input impedance of the dual-resonant circuit of Fig. 1b. It is well known that a positive series reactance shifts all impedances on the Smith chart towards larger inductive reactance values along the constant resistance circles. By using the information given in Figs. 5 and 6, the effect of a typical series reactance can be compensated and the coupling loop can be moved back to the optimal position in the center. For example, in this case ($Q_{01} = Q_{02}$ = 23.9) the effect of the normalized series reactance x = 1 can be compensated by increasing f_{r2} by approximately 7 % (see Fig. 6a, thick dashed line) and by increasing k_1 and k_2 slightly. Another and perhaps a better approach, which leads to the same end result, is the following. It is known that adding an inductive series reactance to a simple parallel resonant circuit increases the frequency at which the magnitude of the input reflection coefficient reaches its minimum. Therefore, by using this frequency as f_{r1} and then by setting $f_{r1} = f_{r2}$, the coupling loop is automatically centered so that it is only necessary to adjust k_1 and k_2 in order to optimize the impedance bandwidth.

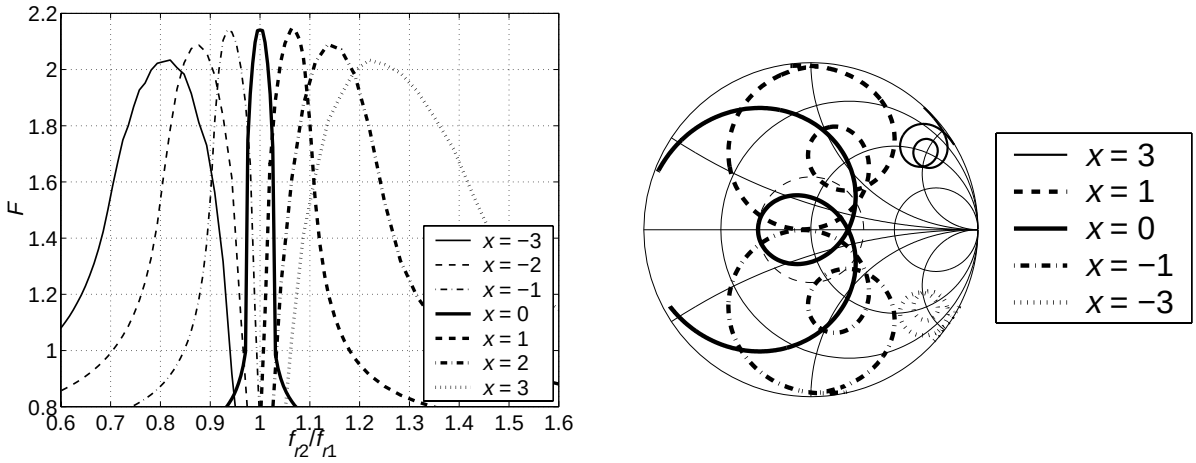

(a) (b)

Figure 6. *a) Bandwidth enhancement factor ($L_{retn} \geq 10$ dB) as a function of f_{r2}/f_{r1} for seven normalized series input reactances (x), ($Q_{01} = Q_{02} = 23.9$, $Q_0 = 14.9$). b) Effect of series input reactance (x) on the input impedance locus of the circuit of Fig. 1b. Values of other parameters: $Q_{01} = Q_{02} = 23.9$, $f_{r1} = f_{r2} = 1$, $k_1 = k_{1,opt} = 1.317 \times 10^{-1}$, and $k_2 = k_{2,opt} = 8.855 \times 10^{-3}$.*

2.6 Equations for Optimal Impedance Bandwidth of Dual-Resonant Antennas

Based on the model of Fig. 1b and the information presented in Sec. 2, it is possible to derive a simple approximate equation for the optimal relative impedance bandwidth of dual-resonant patch antennas ($B_{dr,opt}$). The optimal bandwidth depends only on the unloaded quality factors of the resonators (Q_{01} and Q_{02}) and the maximum allowed voltage standing wave ratio ($VSWR \leq S$). When both Q_{01} and Q_{02} have finite values, the optimal dual-resonant bandwidth can be calculated from

$$B_{dr,opt} = \sqrt{S^2 - 1}\sqrt{\frac{S^2 - 1}{4S^2} \cdot \frac{1}{Q_{01}^2} + \frac{1}{Q_{01}Q_{02}} + \frac{1}{Q_{02}^2}}\,. \tag{6}$$

In the case of a lossless resonant matching circuit, i.e. $Q_{01} = \infty$, Eq. (6) simplifies to

$$B_{dr,opt} = \frac{\sqrt{S^2 - 1}}{Q_{02}}\,. \tag{7}$$

The derivation of Eqs. (6) and (7), which is presented in Appendix A, assumes that $L_p = 0$ and $f_{r1} = f_{r2}$. These assumptions were shown above to give the optimal bandwidth for the model of Fig. 1b. It was also shown above that typical values of L_p have only a minor effect on the optimal bandwidth. Therefore, in typical cases the effect of L_p can be neglected in the

predictions of optimal bandwidth as long as it is kept in mind that this will make the predictions slightly optimistic and that the prediction error increases as L_p increases.

Exchanging the order of the resonant circuits and ideal transformers in the model of Fig. 1b leads to the same equations for optimal bandwidth as Eqs. (6) and (7). Equation (7) has also been obtained in [10] for an open-circuited patch antenna with a series resonant matching circuit. To the authors' knowledge, the more general result given by Eq. (6) has not been published prior to this in open literature. It can be shown that Eqs. (5), (6), and (7) fully agree with the results presented by Fano in [39].

3 Parameter Study for Stacked Shorted Patch Antenna

3.1 MODEL

In this section, the main design parameters concerning the input impedance of a stacked short-circuited patch antenna are discussed to support the theory presented in Sec. 2. To obtain a simulation model for the parameter study, an 8.2 mm-thick stacked shorted patch antenna was first designed using IE3D (Ver. 5.2), which is a commercial method of moments -based 3D full-wave simulation software. The antenna was then constructed and measured to test the simulation model. As shown in Fig. 7a, the measured and the simulated results agree very well. The dimensions of the antenna are given in Fig. 7b (see also Fig. 1a). The patches of the prototype were made from tin bronze ($\sigma = 0.8 \times 10^7$ S/m) and the ground plane from copper ($\sigma = 5.8 \times 10^7$ S/m). The feed probe was gold-plated ($\sigma = 4.1 \times 10^7$ S/m). As a conservative estimate based on [40], the surface roughness of the metals was taken into account by doubling their surface resistance in the simulation model. To reduce the computation time, the antenna model was simulated on an infinite ground plane. In the measurements, the infinite ground plane was approximated by positioning the antenna element on a large 0.5 m × 0.5 m ground plane. Based on the agreement between the simulated and measured results shown in Fig. 7a, it may be assumed that the model predicts changes in the input impedance with sufficient accuracy when the dimensions of the antenna are varied.

As shown in Fig. 7a, a continuous band, where $L_{retn} \geq 10$ dB, was not quite obtained with the dimensions given in Fig. 7b. According to Fig. 7a, there was approximately a 0.5 dB-difference between the simulated and measured results near 1.8 GHz. To obtain the desired match over the joined bandwidths of the two resonances, the dimensions of the antenna model were slightly adjusted, and near 1.8 GHz, a 1 dB-margin was intentionally left to the improved design. Its dimensions are given in Fig. 8d. The improved design is used as the starting point for the parameter study, where it is referred to as the optimized antenna (thick solid line in Figs. 8 and 10). Next, the geometrical parameters of the optimized design are varied one at a time to see their effects on the input impedance.

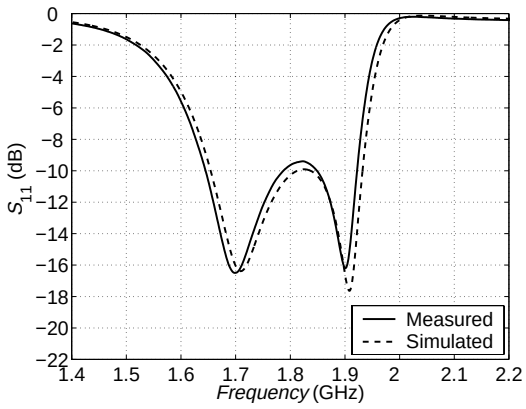

(a)

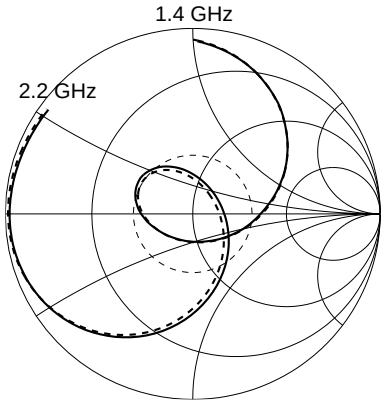

ε_r'	1.0
$\tan\delta$	0
l_1	40.1
l_2	33.5
w_1	30
w_2	30
h_1	3.5
h_2	8.0
w_{s1}	30
w_{s2}	30
d	13.4
t	0.2

(b)

Figure 7. *a) Measured and simulated frequency responses of reflection coefficient for the stacked shorted patch antenna with dimensions given in Fig. 7b. Dashed circle on the Smith chart represents L_{retn} = 10 dB. b) Design parameters for an 8.2 mm-thick stacked shorted patch antenna (t denotes thickness of the patch metal). All dimensions are in millimeters. Diameter of the feed probe is 1.3 mm.*

3.2 RESONANT FREQUENCIES OF PATCHES

Figure 8a shows the impedance behavior of the stacked shorted patch antenna when the length of the lower patch (l_1) is varied in 1 mm steps. As l_1 is decreased from the optimal value of 39.9 mm, the resonant frequency of the lower patch (f_{r1}) increases. This decreases the ratio of the resonant frequencies of the upper and the lower patch (f_{r2}/f_{r1}), which causes the coupling loop to shift from the optimal position (thick solid line) towards the low-frequency end of the impedance locus (dashed line and thin solid line). When l_1 is increased, f_{r1} decreases, f_{r2}/f_{r1} increases, and the coupling loop shifts in the opposite direction, towards the high-frequency end of the impedance locus, as explained in Sec. 2.4 (dashdot and dotted lines).

Figure 8b shows the impedance behavior of the stacked shorted patch antenna when the length of the upper patch (l_2) is varied in 1 mm steps. As l_2 is decreased from the optimal value of 33.4 mm (thick solid line), the resonant frequency of the upper patch increases. This increases f_{r2}/f_{r1} and causes the coupling loop to shift from the optimal position towards the high-frequency end of the impedance locus (dashed line and thin solid line). When l_2 is increased, f_{r2} decreases, f_{r2}/f_{r1} decreases, and the coupling loop shifts towards the low-frequency end of the impedance locus, again as explained in Sec. 2.4 (dashdot and dotted lines).

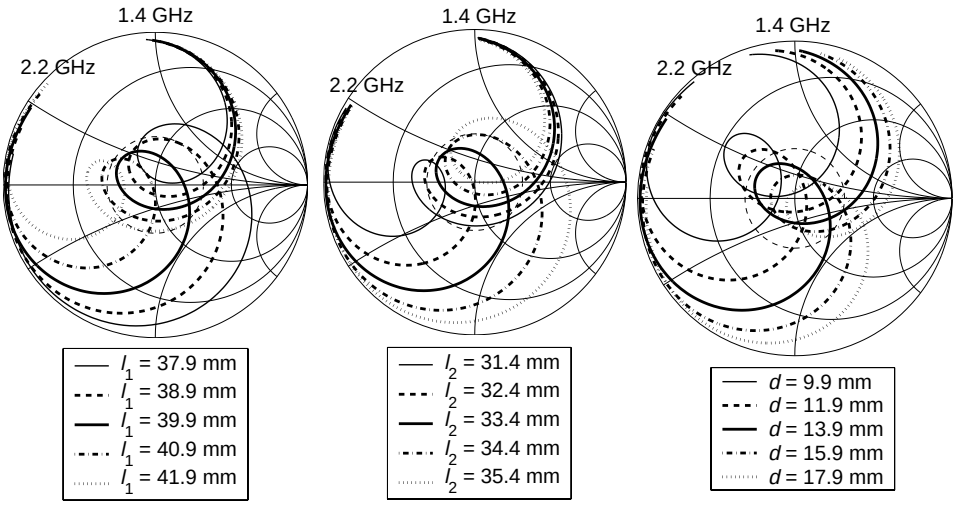

ε_r'	1.0
$\tan\delta$	0
l_1	39.9
l_2	33.4
w_1	30
w_2	30
h_1	3.5
h_2	8.0
w_{s1}	30
w_{s2}	30
d	13.9
t	0.2

(a) (b) (c) (d)

Figure 8. *Effects of three geometrical parameters on the input impedance locus of the optimized stacked shorted patch antenna. a) Effect of lower patch length (l_1). b) Effect of upper patch length (l_2). c) Effect of distance from short circuit to feed probe (d). Dashed circles on the Smith charts represent L_{retn} = 10 dB. d) Design parameters for the optimized stacked shorted patch antenna (thick solid line). Parameter t denotes thickness of the patch metal. All dimensions are in millimeters.*

The shapes of the impedance loci on the Smith chart of Fig. 8a are very similar to those of Fig. 8b. For example, increasing l_1 has a similar effect on the position of the coupling loop as decreasing l_2. Based on Sec. 2.4, this is an expected result because in both cases the ratio f_{r2}/f_{r1} increases. However, there is also a significant difference, i.e., increasing l_1 will decrease the center frequency (f_c) of the whole antenna whereas decreasing l_2 will increase it. Finally, it may be concluded that to obtain a well-tuned dual-resonant stacked shorted patch, i.e., to center the coupling loop, the relative lengths of the patches (and thus f_{r2}/f_{r1}) must be optimized. The same result was also obtained in Sec. 2.4 (Fig. 5a).

3.3 Coupling Between Feed and Driven Patch

Figure 8c shows the impedance behavior of the stacked shorted patch antenna when the coupling between the feed and the driven patch (k_1) is varied by changing the distance from the short circuit to the feed probe (d) in 2 mm steps. The behavior is similar to that of a traditional single-resonant shorted patch antenna and also well described by the model of Fig. 1b in Fig. 5b. The size of the large loop of the impedance locus decreases (k_1 decreases) as the probe is moved towards the shorted edge (dashed and thin solid line) and increases (k_1 increases) as the probe is moved towards the open edge of the patch (dashdot and dotted lines).

3.4 COUPLING BETWEEN PATCHES

As mentioned in Sec. 2, a method of controlling the coupling between the driven and the parasitic patch (i.e. the size of the coupling loop) is needed to optimize the impedance behavior of a dual-resonant patch antenna. The position of the coupling loop should remain as close to the original while its size changes. It seems that the size of the coupling loop of a stacked shorted patch antenna is mainly affected by the separation between the open ends (electric field maximums) of the patches. Thus, the coupling happens mainly through the fringing fields of the patches and can be controlled by moving the upper patch and upper short circuit closer to the open end of the driven patch (Fig. 9a) or further away from it (Fig. 9b). The first case is here called forward offset and the second case backward offset. Backward offset can also be realized with separate shorting elements (Fig. 9c).

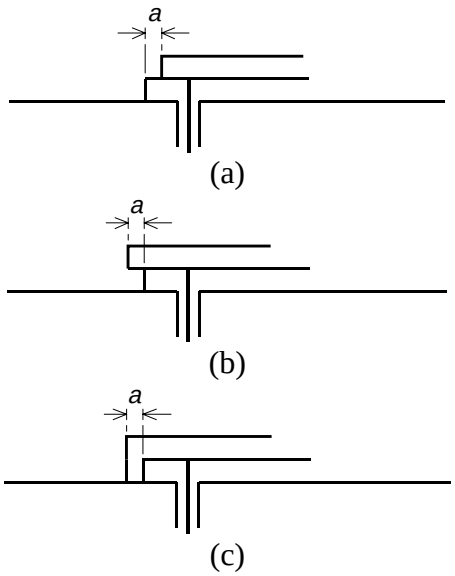

Figure 9. *Stacked shorted patch antenna with offset parasitic: (a) forward offset, (b) backward offset, and (c) backward offset with separate short circuits.*

Figure 10a shows the effects of forward and backward offsets on the input impedance of the stacked shorted patch antenna (see also Fig. 5c). The configurations of Figs. 9a and 9b are used in Fig. 10a. The coupling between the patches decreases, when the open end of the upper patch is moved away from that of the lower patch as in Fig. 9b. At the same time, the coupling loop shifts slightly towards the high-frequency end of the impedance locus indicating a slight increase in f_{r2}. When the open ends of the patches are moved closer to each other, as in Fig. 9a, the coupling between the patches increases. At the same time, f_{r2} decreases slightly. If necessary, the coupling can be further increased from that obtained with the offsets by adding

a narrow metal strip between the patches, as presented in [41] for coplanar patches. The weakest coupling in that case is obtained when the metal strip is between the short circuits. The coupling increases as the strip is moved towards the open ends of the patches. For stacked patches, this method has been used in [15].

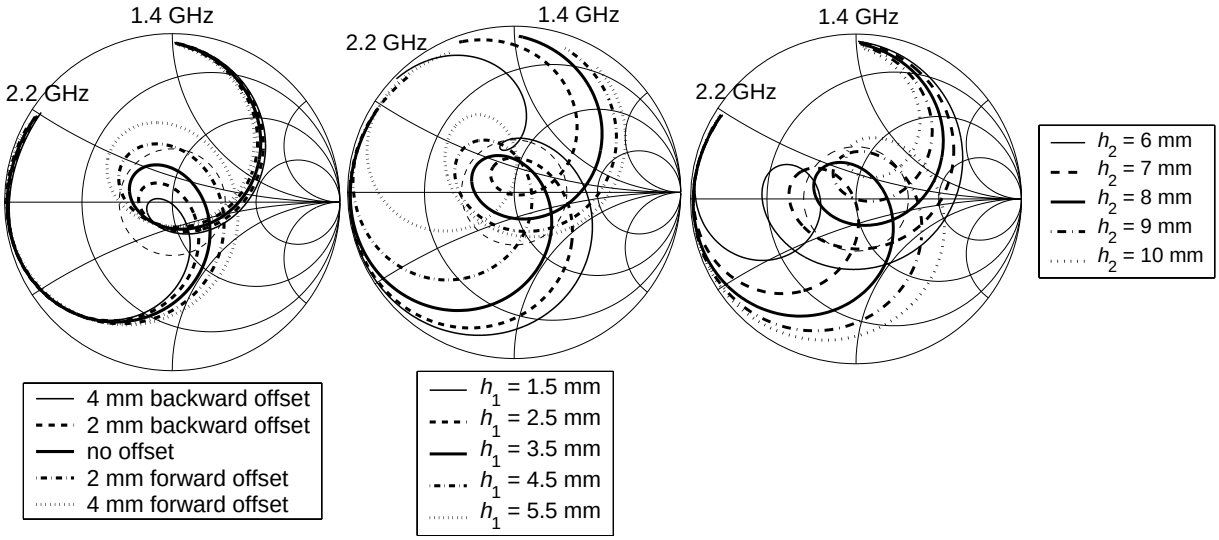

(a) (b) (c)

Figure 10. *Effects of three geometrical parameters on the input impedance locus of the optimized stacked shorted patch antenna. a) Effect of offset between patches (a). b) Effect of lower patch height (h_1). c) Effect of upper patch height (h_2). Dashed circles on the Smith charts represent L_{retn} = 10 dB.*

Another way of affecting the distance between the open ends of the patches is changing the heights of the patches. The effect of the lower patch height (h_1) on the input impedance of the stacked shorted patch antenna is shown in Fig. 10b. When h_1 is decreased from the level selected here as optimal (thick solid line), the size of the coupling loop decreases (dashed line and thin solid line). This indicates a decrease of coupling, which is assumed to be caused mainly by the increasing vertical distance between the open ends of the patches. The loop also shifts towards the low-frequency end of the impedance locus. This happens because f_{r1} increases as h_1 decreases [32] (l_1 is constant). Each time h_1 has been changed, the length of the feed probe has also been changed accordingly. The "rotation" of the whole impedance locus is caused by the change in the probe inductance, which decreases as the probe length decreases. When h_1 is increased, the size of the coupling loop increases (dashdot and dotted lines), the loop shifts towards the high-frequency end of the impedance locus, and the whole locus rotates in the opposite direction as when h_1 was decreased.

The effect of the upper patch height (h_2) on the impedance locus is shown in Fig. 10c. As h_2 decreases, the distance between the open ends decreases and the coupling between the patches increases. At the same time, the coupling loop shifts towards the high-frequency end of the impedance locus (dashed line and thin solid line) because f_{r2} increases as h_2 decreases (l_2 is constant). The size of the coupling loop increases (dashed and thin solid line) only a little because the increase is compensated by the decrease that happens when the loop shifts towards the high-frequency end of the impedance locus (Figs. 8a and 8b). As h_2 is increased from the optimum, the distance between the open ends increases and the coupling between the patches decreases (dashdot and dotted line). The coupling loop shifts towards the low-frequency end of the impedance locus because f_{r2} decreases as h_2 increases.

4 Application Examples

This section presents examples where the model of Fig. 1b and Eqs. (4)–(7) are used to estimate the optimal impedance bandwidths and bandwidth enhancement factors (F) obtained with several dual-resonant patch antenna configurations. As can be observed from Eq. (6), the impedance bandwidth of a dual-resonant patch antenna is the wider, the lower Q_{01} and Q_{02} are. If Q_{01} is infinite and Q_{02} has an arbitrary but finite value, $F = 2.3$ is obtained (bandwidth criterion $L_{retn} \geq 10$ dB or $VSWR \leq 1.92$). If the first resonator can be made to radiate (or has other undesired losses), Q_{01} decreases and F increases. In ideal case, $Q_{01} = Q_{02}$ and $F = 3.5$ ($L_{retn} \geq 10$ dB). With just two radiating resonators, this is already rather close to the ultimate limit of $F_{max} = 3.9$ obtained with an infinitely large lossless matching circuitry [39], [7]. According to [39], an optimized matching circuit comprising at least five additional lossless resonators is needed to obtain $F = 3.5$. Based on the theory presented above, it seems reasonable from the impedance bandwidth point of view to make also the driven resonator radiate as well as possible.

4.1 Dual-Resonant Modified Microstrip Patch Antenna

Without increasing the antenna size, the largest bandwidth enhancement factor that can be obtained with a lossless dual-resonant microstrip patch type of antenna is obtained with an antenna structure where in addition to the fundamental resonance, it is possible to excite another resonance with f_r and Q_0 equal to those of the fundamental resonance. In practice, this can be done by exciting two nearly orthogonal resonant modes in an open-circuited patch in a similar manner as in the design of single feed circularly-polarized patch antennas [42]. Furthermore, the coupling between the resonant modes and the coupling of the feed to the driven mode must be optimized to maximize the bandwidth, as explained in Sec. 2. The antenna studied in [43] is used here as an example of these antenna types. It is noted that here we are concentrating only on the impedance bandwidth. The radiation characteristics of the antenna of [43] change with frequency, thus the pattern properties limit its usefulness in many applications. The model of Fig. 1b can be used to describe only the input impedance of the antenna presented in [43]. The resonant frequencies of the two resonant modes of the antenna are controlled by varying the corresponding lengths of the sides of the patch (l_1 and l_2 in Fig. 11a). The coupling of the feed to the driven mode is controlled by varying the distance from

the center of the probe to the radiating edge of the driven mode (x_p). The coupling between the resonant modes is controlled by varying the size of the square removed from the corner of the patch (d_1 and d_2).

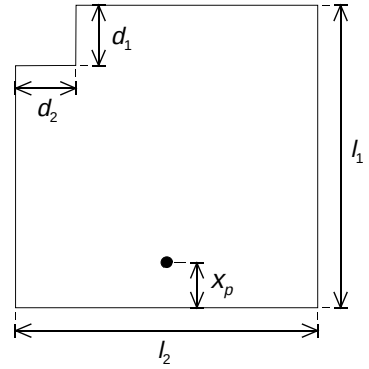

(a)

ε_r	1
$\tan\delta$	0
l_1	76.6
l_2	76.6
d_1	0
d_2	0
h	3
x_p	23.8
t	0.2

(b)

ε_r	1
$\tan\delta$	0
l_1	79.5
l_2	78.2
d_1	16.2
d_2	16.2
h	3
x_p	11.1
t	0.2

(c)

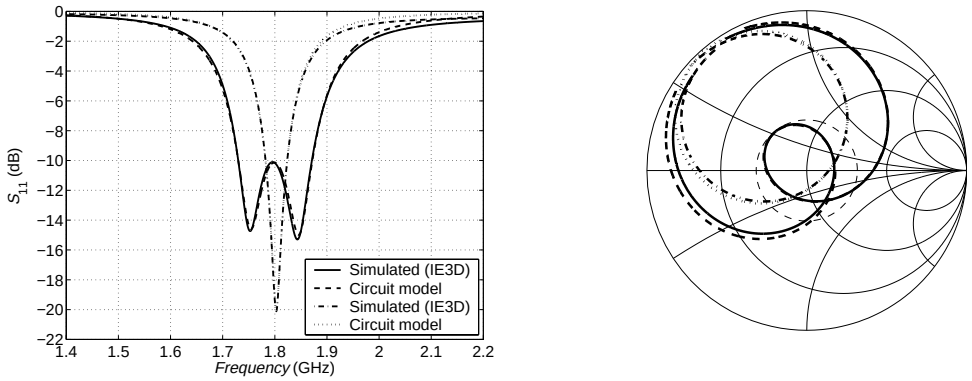

(d)

Figure 11. *a) Geometry of a microstrip patch antenna. Dimensions (in millimeters) for optimized b) single-resonant and c) dual-resonant microstrip patch antennas. Probe diameter is 1.3 mm in both cases. d) Frequency responses of reflection coefficient for optimized dual-resonant and single-resonant patches. Component values for the equivalent circuit of single-resonant antenna: L_p = 2.11 nH, k_1 = 1, C_1 = 36.95 pF, L_1 = 0.2149 nH, G_1 = 13.51 mS (Z_0 = 50 Ω). Component values for the equivalent circuit of dual-resonant antenna: L_p = 2.11 nH, $k_1 = 1.271 \times 10^{-3}$, C_1 = 1.814 pF, L_1 = 4.535 nH, G_1 = 0.652 mS, $k_2 = 5.375 \times 10^{-3}$, C_2 = 1.769 pF, L_2 = 4.423 nH, and R_2 = 1.630 Ω (Z_0 = 50 Ω).*

According to a simulation with IE3D, a probe-fed open-circuited microstrip patch antenna with the size 76.6 mm × 76.6 mm × 3 mm (*length* × *width* × *height*) has the Q_0 = 30.7 (and $B_{sr,opt}$ = 2.3 %) at f_c = 1803 MHz (all dimensions in Figs. 11a and 11b). Using this value for the two resonant modes (Q_{01} = Q_{02} = 30.7), the optimal relative bandwidth of $B_{dr,opt}$ = 7.9 % and a bandwidth enhancement factor of F = 3.5 are estimated for the optimized dual-resonant antenna with Eqs. (4)–(6). A dual-resonant patch as described above was designed and optimized with IE3D using the methods presented in Secs. 2 and 3. The optimal simulated

bandwidth for the antenna was $B_{dr,opt}$ = 7.9 % and F = 3.4, which agree very well with the calculated results. The optimized antenna structure and its dimensions are shown in Figs. 11a and 11c, respectively. The simulated frequency responses of the reflection coefficient for the optimized single-resonant and dual-resonant patch antennas are shown in Fig. 11b. Based on the simulated data and the model of Fig. 1b, equivalent circuits for both antennas were extracted. The component values are given in the caption of Fig. 11. The frequency responses of the reflection coefficient for the equivalent circuits are also given in Fig. 11d. The agreement between the equivalent circuit models and simulations is excellent.

4.2 Comparison of Three Dual-Resonant Shorted Patch Antenna Structures

In the second example, the model of Fig. 1b and Eqs. (4)–(7) are used to compare the bandwidth enhancement factors obtained by replacing a simple shorted patch antenna with three different dual-resonant shorted patch antenna configurations. All the antennas have the same overall shape and thus occupy an equal volume ($l \times w \times h$ = 40 mm × 30 mm × 8 mm). The comparison is based on data obtained from [32]. The structures to be compared are: a stacked shorted patch, a shorted patch with a coplanar parasitic patch, and a shorted patch with a high-Q matching resonator. It is assumed for the bandwidth estimation that the Q_0 of an isolated shorted patch antenna can be used to approximate that of the same patch with another patch positioned in its proximity. The Q_0s for the patches are obtained from Fig. 5.9 of [32] by converting the given bandwidth values with S = 1.5 using the well-known equation [44], [7]

$$Q_0 = \frac{S-1}{\sqrt{S}B_r}. \tag{8}$$

The equation is valid for perfectly matched antennas. Although not mentioned in [32], it is reasonable to assume that the data given in Fig. 5.9 of [32] is for perfectly matched antennas. The assumption is supported by the close agreement of the data in Fig 5.9 of [32] and a few test simulations. The width-to-length ratios (w/l) of the patches of the simple shorted patch antenna and the stacked shorted patch antenna were 0.75. The bandwidth values used for the calculation of Q_0s were taken as the average of the values read from the curves representing w/l = 0.5 and w/l = 1. The shorted patch with the coplanar parasitic was obtained by dividing the single-resonant reference antenna into two narrower patches with equal widths (w/l = 0.375). The bandwidth values used for the calculation of Q_0s were taken as the average of the values read from the curves representing w/l = 0.25 and w/l = 0.5. In reality, a narrow gap is also needed between the patches. However, because it is very difficult to estimate the

necessary gap width, which is typically fairly small, it is not taken into account here. As a result of this, the bandwidth of this structure will be slightly overestimated. For the shorted patch with a high-Q matching resonator, Q_{02} was approximated from Fig. 5.9 of [32] and Q_{01} was set infinite ($G_1 = 0$).

The antenna structures were also simulated with IE3D for comparison. In the simulations, the optimized stacked shorted patch was obtained by moving the feed probe of the antenna presented in Sec. 3 (structure in Fig. 1a) 0.5 mm towards the short circuit (d = 13.4 mm). The other dimensions are those given in Fig. 8d. The structure of the shorted patch with a coplanar parasitic and its dimensions are given in Fig. 12a. Near the short circuits, the patches are galvanically connected by a narrow metal strip to increase the coupling between them [41] so that the bandwidth could be optimized. The patches have separate short circuits, which have the same widths as the patches. The structure of the simulated shorted patch with a lossless matching circuit is given in Fig. 12b. The lossless matching resonator was approximated with a narrow section of short-circuited transmission line. The calculated and simulated bandwidth enhancement factors for the different structures and the width-to-length ratios, heights, and Q_0s of the patches used in the calculations are given in Table 1.

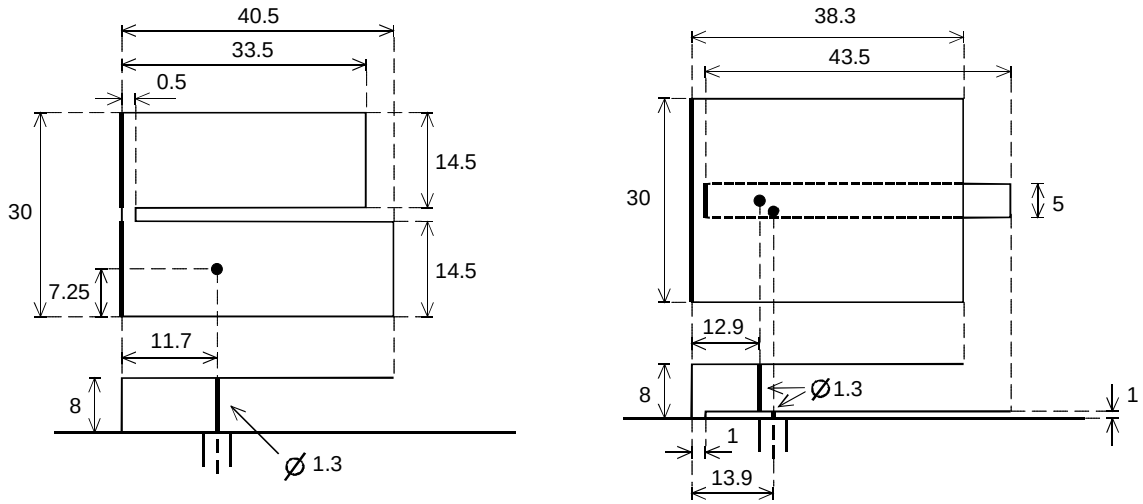

Figure 12. *Geometries of a) the shorted patch with a coplanar parasitic patch and b) the shorted patch with a matching resonator. All dimensions are in millimeters.*

As shown in Table 1, the model predicts very well the bandwidth enhancement factor for the case of the shorted patch with a high-Q matching resonator whereas the simulated values for the shorted patch with a coplanar parasitic patch and the stacked shorted patch are clearly lower than predicted. The reasons for this are explained next.

Table 1. *Comparison of calculated and simulated bandwidth enhancement factors for three dual-resonant shorted patch antennas and heights, width-to-length ratios, and unloaded quality factors used in the calculations. Bandwidth criterion is $L_{retn} \geq 10$ dB, and center frequency is $f_c = 1.8$ GHz.*

	Shorted patch	**Stacked shorted patch**	**Shorted patch with coplanar parasitic**	**High-*Q* matching resonator**
$\boldsymbol{h_1}$ **(**$\boldsymbol{\lambda_0}$**)**	-	0.021	0.048	-
$\boldsymbol{h_2}$ **(**$\boldsymbol{\lambda_0}$**)**	0.048	0.048	0.048	0.048
$\boldsymbol{w_1/l_1}$	-	0.75	0.38	-
$\boldsymbol{w_2/l_2}$	0.75	0.75	0.38	0.75
$\boldsymbol{Q_{01}}$	-	28.7	14.9	∞
$\boldsymbol{Q_{02}}$	9.8	9.8	14.9	9.8
Calculated $\boldsymbol{F_{max}}$	-	**2.7**	**2.3**	**2.3**
Simulated $\boldsymbol{F_{max}}$	-	**1.9**	**1.6**	**2.1**

Based on the simulated input impedance, the unloaded quality factors $Q_{01} = 28.7$ and $Q_{02} = 9.8$, and the model of Fig. 1b (including L_p), an equivalent circuit for the stacked shorted patch antenna was obtained. The values of the other parameters of the model are: $L_p = 1.9$ nH, $G_1 = 0.697$ mS, $L_1 = 4.547$ nH, $C_1 = 1.819$ pF, $R_2 = 5.102$ Ω, $L_2 = 4.360$ nH, $C_2 = 1.744$ pF, $k_1 = 2.404 \times 10^{-1}$, and $k_2 = 3.591 \times 10^{-2}$ ($f_{r1} = 1.750$ GHz, $f_{r2} = 1.825$ GHz, and $Z_0 = 50$ Ω). Fig. 13 shows a comparison of the reflection coefficients obtained for the antenna with IE3D and with the circuit model. The bandwidth given by the model is significantly wider than that of the real antenna. Some of the difference may be attributed to the approximation of the Q_0s. Part of it, however, is due to the transmission zero at about 2.04 GHz. As shown by the realized maximum gain (G_{max}) in Fig. 13, around this frequency the antenna almost stops radiating, which is also seen in the reflection coefficient (S_{11}) and in the radiation efficiency (η_r). At 2.04 GHz there is a nearly perfect short circuit at the antenna input. Similar phenomenon, which is most likely caused by a non-radiating almost degenerate resonant mode, has been noticed by the authors in open-circuited and in shorted patches with both coplanar and stacked parasitics. Depending on the configuration, this mode typically appears either above or below the desired resonances. Its resonant frequency seems to be related to the dimensions of the slot between the patches. In the proximity of this resonant mode, the radiation patterns have also been noticed to change considerably. Typically, electrically thin lower substrates have been used in stacked open-circuited patches to minimize surface wave excitation. This, together with an electrically thick upper substrate, has inherently alleviated the problem, which explains why there is very little published information available on the

subject. Prior to this paper, the non-radiating mode has been noticed in thick multiresonant patches in [45]. In [46], it was called the odd mode because in its proximity the currents of the patches are out of phase. In stacked patches, the effect of the non-radiating mode seems to be the stronger, the closer the patches are to each other.

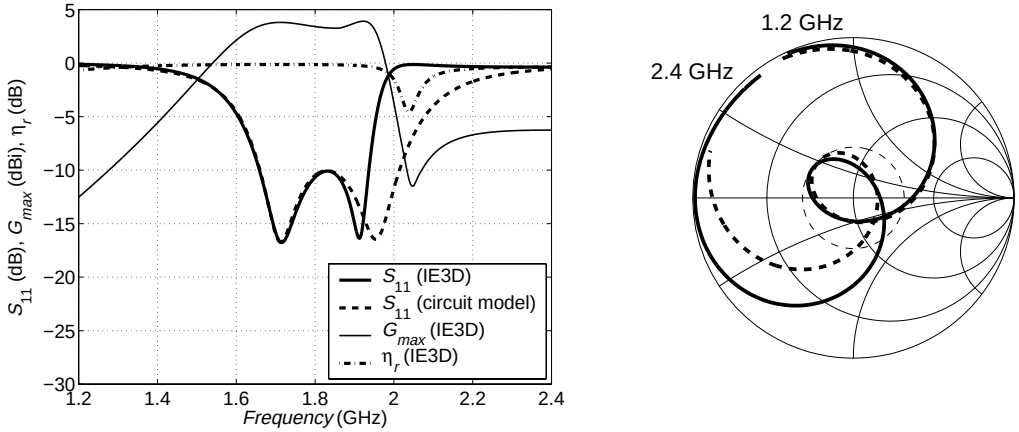

Figure 13. *Comparison of reflection coefficients obtained for the stacked shorted patch antenna with IE3D and with the circuit model of Fig. 1b. Realized maximum gain (G_{max}) and radiation efficiency (η_r) are also given for the antenna simulated with IE3D.*

Figure 14 shows the simulated frequency responses of reflection coefficient, realized maximum gains, and radiation efficiencies for the shorted patch with a coplanar parasitic and for the shorted patch with a high-*Q* matching resonator. Similar asymmetry and a poorly radiating resonance as with the stacked shorted patch can be observed in the case of a shorted patch with a coplanar parasitic. In this case, the resonant frequency of the undesired mode is lower (about 1.97 GHz) causing *F* to be smaller than in the case of the stacked shorted patch.

In practice, the use of a high-Q matching resonator turned out to be the most effective of the three compared bandwidth enhancement methods. The frequency responses of the shorted patch with a high-*Q* matching resonator are significantly more symmetrical, and the calculated and simulated bandwidth enhancement factors agree better than in the cases of stacked and coplanar parasitics even though the antenna structure is in principle almost the same as that of the stacked shorted patch. This is because the resonant frequency of the undesired mode is higher (near 2.4 GHz) and the patches are further apart. However, the undesired mode may still partly explain the minor difference between the calculated and simulated bandwidth enhancement factors. This case shows that the frequency of the undesired resonant mode can be affected and moved outside the frequency range of interest to minimize its effect and to maximize the bandwidth in some cases.

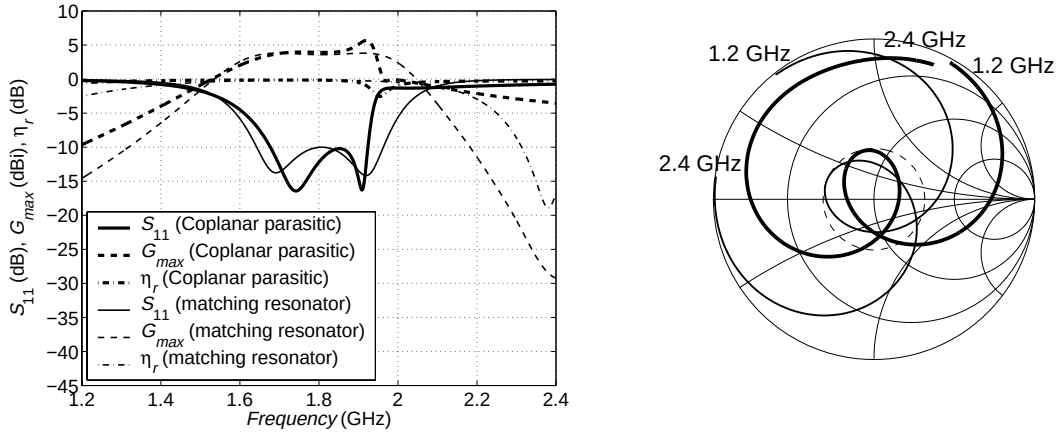

Figure 14. *Frequency response of reflection coefficient, realized maximum gain, and radiation efficiency for the shorted patch with a coplanar parasitic patch (thick lines) and for the shorted patch with a high-Q matching resonator (thin lines).*

In all the examples presented above, the antenna element was positioned on top of large ground plane, which could be approximated in the simulations with an infinite ground plane to reduce the computation time. The use of the large ground plane also enabled the use of *Q*-values obtained from the literature as the basis for bandwidth prediction. At the moment, short-circuited microstrip patch antennas (and PIFAs) are mainly used as internal antennas in mobile phones, where the antenna is located on an infinite ground plane. It is well known that performance of internal handset antennas depends strongly on the dimensions of this ground plane and the position of the antenna on it [32], [47]–[49]. For this reason, *Q*-values obtained on large or infinite ground plane cannot be used to predict the impedance bandwidth of the same antenna positioned on a finite ground plane. This applies to the bandwidth prediction of single-resonant antennas using Eqs. (5) and (8) as well as to the bandwidth prediction of dual-resonant antennas using Eqs. (6) and (7). However, for an antenna that is attached to a finite ground plane, it is in most cases possible to determine an effective unloaded quality factor ($Q_{0,eff}$), which takes into account the effect of the finite ground plane. The impedance bandwidth of antennas on finite ground planes can be calculated by using $Q_{0,eff}$ instead of Q_0 in Eqs. (5)–(8). An example of a dual-resonant shorted patch with a coplanar parasitic on a finite ground plane has been presented by the authors in [50]. It was shown that by dividing a patch into two properly tuned narrow strips, of which one was driven and the other one was parasitic, the impedance bandwidth could be increased by a factor of 2.2 without increasing the size of the antenna. The obtained value is of the same order as the typical bandwidth enhancement factors that can be predicted based on literature values for similar antennas on large ground planes, such as the shorted patch with a coplanar parasitic studied in this section.

5 Conclusions

The design of dual-resonant patch antennas was discussed with the emphasis on the bandwidth optimization and prediction. The most important electrical design parameters concerning the optimization of impedance bandwidth were systematically analyzed with a simplified dual-resonant lumped-element circuit model. It was shown that the main electrical design parameters are the Q_0s and the relative resonant frequencies of the patches, the coupling of the feed to the driven patch, and the coupling between the patches. The Q_0s of the patches define the bandwidth potential of the antenna, whereas the other mentioned parameters are used to optimize the impedance behavior so that the maximum bandwidth, defined by the Q_0s, can be obtained. In parameter studies for the circuit model and for a real stacked shorted patch antenna, it was shown how the main electrical design parameters affect the input impedance and how they are used to optimize the impedance bandwidth. Although the paper concentrates on microstrip patch antennas, the main ideas of the presented design methods can also be applied to other narrow-band resonant antennas with only minor modifications.

Novel simple equations enabling quality factor based predictions of optimal impedance bandwidth of dual-resonant patch antennas were also derived in the paper. The equations were shown to give excellent results in cases where only two resonant modes were within the frequency range of interest. Furthermore, comparison of the model and practical antennas revealed the existence of an undesired non-radiating resonant mode near the two desired radiating resonances in patch antennas having a stacked or coplanar parasitic patch. The undesired mode decreases the impedance bandwidth of some dual-resonant structures and causes the circuit model to overestimate it. This decrease of bandwidth is difficult to estimate because it depends on the configuration. However, despite the non-radiating resonance, the simple model and the equations given in Appendix A can be used to estimate an upper limit for the impedance bandwidth, i.e. if the bandwidth predicted by the model is not sufficient, the Q_0s of the resonators should be decreased e.g. by increasing antenna height. Although, the used model describes the basic dual-resonant behavior of the studied antennas very well, as shown in Secs. 2 and 3, it is obvious that a slightly more complicated model (with at least one additional high-Q resonator) is needed to properly model also the undesired mode.

6 Acknowledgements

This work has been partly financed by the Graduate School in Electronics, Telecommunications, and Automation (GETA), the Academy of Finland, and Finnish telecommunications industry together with the National Technology Agency of Finland (TEKES). Financial support from Jenny and Antti Wihuri Foundation, Tekniikan Edistämissäätiö (TES), the Finnish Society of Electronics Engineers (EIS), Nokia Foundation, and Ulla Tuominen Foundation is also gratefully acknowledged.

References

[1] A. Henderson, J. R. James, C. M. Hall, "Bandwidth extension techniques in printed conformal antennas," *Proc. Military Microwaves Conference '86*, Brighton, England, June 1986, pp. 329-334.

[2] D. H. Schaubert, "Multilayer and parasitic configurations," Chapter 6 in *Handbook of Microstrip Antennas, Vol. I*, J. R. James and P. S. Hall, (Editors), London, 1989, Peter Peregrinus, 813 p.

[3] D. M. Pozar, "Microstrip antennas," *Proceedings of the IEEE*, Vol. 80, No. 1, Jan. 1992, pp. 79-91.

[4] J. R. James and P. S. Hall, "Introduction," Chapter 1 in *Handbook of Microstrip Antennas, Vol. I*, J. R. James and P. S. Hall, (Editors), London, 1989, Peter Peregrinus, 813 p.

[5] H. A. Wheeler, "Small Antennas," *IEEE Transactions on Antennas and Propagation*, Vol. AP-23, No. 4, July 1975, pp. 462-469.

[6] D. M. Pozar and B. Kaufman, "Increasing the bandwidth of a microstrip antenna by proximity coupling," *Electronics Letters*, Vol. 23, No. 8, Mar. 1987, pp. 368-369.

[7] H. F. Pues and A. R. Van de Capelle, "An impedance matching technique for increasing the bandwidth of microstrip antennas," *IEEE Transactions on Antennas and Propagation*, Vol. AP-37, No. 11, Nov. 1989, pp. 1345-1354.

[8] N. C. Karmakar and M. E. Bialkowski, "On the modeling of a cavity enclosed broadband circular patch antenna for L-band land mobile satellite communications," *Microwave and Optical Technology Letters*, Vol. 7, No. 17, Dec. 1994, pp. 784-787.

[9] V. Voipio, J. Ollikainen, and P. Vainikainen, "Quarter-wave patch antenna with 35% bandwidth," *IEEE Antennas and Propagation Society International Symposium Digest*, Vol. 2, Atlanta, Georgia, USA, June 21-26, 1998, pp. 790-793.

[10] J. Anguera, C. Puente, J. Romeu, C. Borja, and G. Font, "An optimum method to design probe-fed single-layer single-patch wideband microstrip antenna," *Proc. AP2000 Millennium Conference on Antennas & Propagation*, Davos, Switzerland, Apr. 9-14, 2000, CD-ROM SP-444 (ISBN 92-9092-776-3), paper p1023.pdf.

[11] D. A. Paschen, "Practical examples of integral broadband matching of microstrip antenna elements," *Proc. 1986 Antenna Applications Symposium*, Allerton Park, Illinois, USA, 1986, pp. 199-217.

[12] A. Sabban, "A new broadband stacked two-layer microstrip antenna," *IEEE Antennas and Propagation Society International Symposium Digest*, Houston, Texas, USA, May 23-26, 1983, pp. 63-66.

[13] F. Croq and D. M. Pozar, “Millimeter-wave design of wideband aperture-coupled stacked microstrip antennas,” *IEEE Transactions on Antennas and Propagation*, Vol. AP-39, No. 12, Dec. 1991, pp. 1770-1776.

[14] J. Ollikainen, *Multiresonant Small Planar Antennas*, Master’s Thesis, Helsinki University of Technology, Radio Laboratory, Espoo, Mar. 1997, 128 p.

[15] R. B. Waterhouse, “Broadband stacked shorted patch,” *Electronics Letters*, Vol. 35, No. 2, Jan. 1999, pp. 98-100.

[16] J. Ollikainen, M. Fischer, and P. Vainikainen, “Thin dual-resonant stacked shorted patch antenna for mobile communications,“ *Electronics Letters*, Vol. 35, No. 6, Mar. 1999, pp. 437-438.

[17] L. Zaïd, G. Kossiavas, J.-Y. Dauvinac, J. Cazajous, and A. Papiernik, “Dual-frequency and broad-band antennas with stacked quarter wavelength elements,” *IEEE Transactions on Antennas and Propagation*, Vol. AP-47, No. 4, Apr. 1999, pp. 654-660.

[18] D. H. Schaubert and F. G. Farrar, “Some conformal, printed circuit antenna designs,” *Proc. Workshop on Printed Circuit Antenna Technology,* New Mexico State University, Las Cruces, New Mexico, USA, Oct. 1979, pp. 5/1-21.

[19] C. Wood, “Improved bandwidth of microstrip antennas using parasitic elements,” *IEE Proceedings - Microwaves Antennas and Propagation*, Vol. 127, Pt. H, No. 4, Aug. 1980, pp. 231-234.

[20] G. Kumar and K. C. Gupta, “Broad-band microstrip antennas using additional resonators gap-coupled to the radiating edges,” *IEEE Transactions on Antennas and Propagation*, Vol. AP-32, No. 12, Dec. 1984, pp. 1375-1379.

[21] J. Rasinger, A. L. Scholtz, W. Pichler, and E. Bonek, “A new enhanced bandwidth internal antenna for portable communication systems,” *Proc. 40th IEEE Vehicular Technology Conference*, Orlando, Florida, USA, May 6-9, 1990, pp. 7-12.

[22] J. Rasinger, Die strahlungsgekoppelte Doppelwinkel-Antenne – eine neuartige interne Antenne für mobile Funkgeräte (Radiation-Coupled Dual-L Antenna for Mobile Radio Equipment in German), Doctoral Thesis (Part I), Vienna University of Technology, Faculty of Electrical Engineering, Austria, June 1990, 67 p.

[23] J. Fuhl, P. Nowak, and E. Bonek, “Improved internal antenna for hand-held terminals,” *Electronics Letters*, Vol. 30, No. 22, Sept. 1994, pp. 1816-1818.

[24] F. Croq and A. Papiernik, “Large bandwidth aperture-coupled microstrip antenna,” *Electronics Letters*, Vol. 26, No. 16, Aug. 1990, pp. 1293-1294.

[25] R. B. Waterhouse, “Design of probe-fed stacked patches,” *IEEE Transactions on Antennas and Propagation*, Vol. AP-47, No. 12, Dec. 1999, pp. 1780-1784.

[26] J. Ollikainen and P. Vainikainen, ”Design of dual-resonant patch antennas,” *Proc. 4th European Personal Mobile Communications Conference (EPMCC 2001)*, Vienna, Austria, Feb. 20-22, 2001, CD-ROM (ISBN 3-85133-023-4), paper pap108.pdf.

[27] G. Kumar and K. C. Gupta, “Nonradiating edges and four edges gap-coupled multiple resonator broad-band microstrip antennas,” *IEEE Transactions on Antennas and Propagation*, Vol. AP-33, No. 2, Feb. 1985, pp. 173-178.

[28] K. L. Virga and Y. A. Rahmat-Samii, “Low-profile enhanced bandwidth PIFA antennas for wireless communications packaging,” *IEEE Transactions on Microwave Theory and Techniques*, Vol. MTT-45, No. 10, Oct. 1997, pp. 1879-1888.

[29] H. A. Wheeler, ”Fundamental limitations of small antennas,” *Proceedings of the IRE*, Dec. 1947, pp. 1479-1484.

[30] J. S. McLean, “Re-examination of the fundamental limits on the radiation *Q* of electrically small antennas,” *IEEE Transactions on Antennas and Propagation*, Vol. 44, No. 5, May 1996, pp. 672-676.

[31] W. F. Richards, Y. T. Lo, and D. D. Harrison, “An improved theory for microstrip antennas and applications,” *IEEE Transactions on Antennas and Propagation*, Vol. AP-29, No. 1, Jan. 1981, pp. 38-46.

[32] T. Taga, “Analysis of planar inverted-F antennas and antenna design for portable radio equipment,” Chapter 5 in *Analysis, Design, and Measurement of Small and Low-Profile Antennas*, K. Hirasawa and M. Haneishi, (Editors), Boston, 1992, Artech House, 270 p.

[33] J. Ollikainen, *Multiresonant Low-Profile Internal Antennas for Handsets*, Licentiate Thesis, Helsinki University of Technology, Radio Laboratory, Espoo, Finland, Mar. 2000, 83 p.

[34] J. Anguera, C. Puente, and C. Borja, “A procedure to design wide-band electromagnetically-coupled stacked microstrip antennas based on a simple network model,” *IEEE Antennas and Propagation Society International Symposium Digest*, Vol. 2, Orlando, Florida, USA, July 11-16, 1999, pp. 944-947.

[35] J. Anguera, C. Puente, and C. Borja, “A procedure to design stacked microstrip patch antennas based on a simple network model,” *Microwave and Optical Technology Letters*, Vol. 30, No. 3, Aug. 5, 2001, pp. 149-151.

[36] D. Kajfez, “Dual resonance,” *IEE Proceedings - Microwaves Antennas and Propagation*, Vol. 135, Pt. H, No. 2, Apr. 1988, pp. 141-144.

[37] D. M. Pozar, *Microwave Engineering*, 2. Edition, New York, 1998, John Wiley & Sons, 716 p.

[38] Y. Suzuki and T. Chiba, “Designing method of microstrip antenna considering the bandwidth,” *Transactions of the IECE of Japan*, Vol. E 67, No. 9, Sept. 1984, pp. 488-493.

[39] R. M. Fano, “Theoretical limitations on the broadband matching of arbitrary impedances,” *Journal of the Franklin Institute*, Vol. 249, No. 1, Jan. 1950, pp. 57-83, and No. 2, Feb. 1950, pp. 139-154.

[40] T. C. Edwards, *Foundations for Microstrip Circuit Design*, New York, John Wiley & Sons, 1981, 265 p.

[41] R. Kapur and G. Kumar, “Hybrid-coupled shorted rectangular microstrip antennas,” *Electronics Letters*, Vol. 35, No. 18, Sept. 1999, pp. 1501-1502.

[42] M. Haneishi and Y. Suzuki, “Circular polarization and bandwidth,” Chapter 4 in *Handbook of Microstrip Antennas, Vol. I*, J. R. James and P. S. Hall, (Editors), London, 1989, Peter Peregrinus, 813 p.

[43] M. Rahman and M. A. Stuchly, “Dual-polarization broadband patch antenna,” *Microwave and Optical Technology Letters*, Vol. 22, No. 6, Sept. 20, 1999, pp. 414-420.

[44] K. R. Carver and J. W. Mink, “Microstrip antenna technology,” *IEEE Transactions on Antennas and Propagation*, Vol. AP-29, No. 1, Jan. 1981, pp. 2-24.

[45] S. D. Targonski, R. B. Waterhouse, and D. M. Pozar, “Design of wide-band aperture-stacked patch microstrip antennas,” *IEEE Transactions on Antennas and Propagation*, Vol. AP-46, No. 9, Sept. 1998, pp. 1245-1251.

[46] R. Garg, P. Bhartia, I. Bahl, and A. Ittipiboon, *Microstrip Antenna Design Handbook*, Norwood, 2001, Artech House, 845 p.

[47] T. Taga and K. Tsunekawa, “Performance analysis of a built-in planar inverted F antenna for 800 MHz band portable radio units,” *IEEE Journal on Selected Areas in Communications*, Vol. SAC-5, No. 5, June 1987, pp. 921-929.

[48] P. Vainikainen, J. Ollikainen, O. Kivekäs, and I. Kelander, *Effect of phone chassis on handset antenna performance*, Helsinki University of Technology, Radio Laboratory, Report S240, (ISBN 951-22-4928-6), Espoo, Finland, March 2000, 13 p.

[49] P. Vainikainen, J. Ollikainen, O. Kivekäs, and I. Kelander, ”Resonator-based analysis of the mobile handset antenna and chassis,” *accepted for publication in IEEE Transactions on Antennas and Propagation.*

[50] J. Ollikainen and P. Vainikainen, “Radiation and bandwidth characteristics of two planar multistrip antennas for mobile communication systems,” *Proc. 48th IEEE Vehicular Technology Conference (VTC’98)*, Vol. 2, Ottawa, Ontario, Canada, May 18-21, 1998, pp. 1186-1190.

Appendix A – Derivation of Equations for Optimal Impedance Bandwidth of Dual-Resonant Antennas

When $L_p = 0$ the input impedance of the circuit of Fig. 1b is

$$Z_{in} = \frac{k_1}{G_1 + \mathrm{j}\omega C_1 + \dfrac{1}{\mathrm{j}\omega L_1} + \dfrac{k_2}{R_2 + \mathrm{j}\omega L_2 + \dfrac{1}{\mathrm{j}\omega C_2}}}, \tag{A1}$$

where $k_1 = N_1^2$ and $k_2 = N_2^2$. The component values of the parallel and series resonant circuit of Fig. 1b and Eq. (A1) are related to the unloaded quality factors (Q_0) of the resonators as given by Eqs. (A2) and (A3), respectively [37]:

$$Q_{01} = \frac{\omega_{r1} C_1}{G_1} = \frac{1}{G_1 \omega_{r1} L_1}, \tag{A2}$$

$$Q_{02} = \frac{\omega_{r2} L_2}{R_2} = \frac{1}{R_2 \omega_{r2} C_2}. \tag{A3}$$

The angular resonant frequencies of the resonators (ω_{r1} and ω_{r2}) are calculated from

$$\omega_{ri} = \frac{1}{\sqrt{L_i C_i}}. \tag{A4}$$

By setting $\omega_{r1} = \omega_{r2} = 1$ and by using Eqs. (A2)-(A4), Eq. (A1) can be written as

$$Z_{in} = \frac{k_1}{G_1 + \mathrm{j}\dfrac{1}{L_1}\left(\omega - \dfrac{1}{\omega}\right) + \dfrac{k_2}{R_2 + \mathrm{j}L_2\left(\omega - \dfrac{1}{\omega}\right)}}. \tag{A5}$$

The relative bandwidth B_r is calculated from

$$B_r = \frac{\omega_2 - \omega_1}{\omega_c}, \tag{A6}$$

where the center frequency ω_c is calculated from

$$\omega_c = \sqrt{\omega_1 \omega_2}. \tag{A7}$$

By normalizing to $\omega_c = 1$ and by using Eqs. (A6) and (A7), Eq. (A5) at the angular frequency $\omega = \omega_2$ can be written

$$Z_{in} = \frac{k_1}{G_1 + \mathrm{j}\dfrac{B_r}{L_1} + \dfrac{k_2}{R_2 + \mathrm{j}B_r L_2}}. \tag{A8}$$

The input reflection coefficient of the model is

$$\Gamma = \frac{Z_{in} - Z_0}{Z_{in} + Z_0}. \tag{A9}$$

On the other hand, its absolute value can be written

$$\left|\Gamma\right| = \frac{S-1}{S+1}, \tag{A10}$$

where S is the maximum allowed voltage standing wave ratio (*VSWR*). By normalizing the reference impedance level ($Z_0 = 1$) and the inductances ($L_1 = L_2 = 1$) and by using Eqs. (A8)–(A10), the relative bandwidth as a function of k_1 and k_2 (G_1, R_2, and S are fixed parameters) can be written as

$$B_r = \sqrt{\frac{A + \sqrt{4S\left[R_2\left(G_1 S - k_1\right) + k_2 S\right]\left[R_2\left(k_1 S - G_1\right) - k_2\right] + A^2}}{2S}}, \text{ where} \tag{A11}$$

$$A = G_1 k_1\left(S^2 + 1\right) - S\left(G_1^2 + R_2^2 + k_1^2 - 2k_2\right).$$

This can be used when

$$\frac{k_1 R_2}{S} - G_1 R_2 \le k_2 \le k_1 R_2 S - G_1 R_2. \tag{A12}$$

In its range of validity, Eq. (A11) can be used e.g. to generate plots similar to the one in Fig. 4b. Based on the calculated result shown in Fig. 3a, to optimize the bandwidth, the input impedance must be $Z_{in} = Z_0/S$ at the center frequency $\omega = \omega_c = 1$. Substitution of the normalized ($Z_0 = 1$) input impedance $Z_{in} = 1/S$ and $\omega = \omega_c = 1$ into Eq. (A5) and solving for k_1 gives

$$k_1 = \frac{k_2 + G_1 R_2}{R_2 S}. \tag{A13}$$

Substitution of Eq. (A13) into Eq. (A11) gives the relative bandwidth as a function of k_2 (G_1, R_2, and S are fixed)

$$B_r = \frac{\sqrt{k_2 R_2\left[G_1\left(S^2 - 1\right) + 2S^2 R_2\right] - S^2 R_2^4 - k_2^2}}{S R_2}. \tag{A14}$$

This is valid when the expression under the square root is positive. Equation (A14) can be used e.g. to plot graphs similar to the one in Fig. 4c. The optimal coupling coefficient $k_{2,opt}$ can be obtained by differentiating Eq. (A14) with respect to k_2, by equating the derivative to zero, and by solving for k_2. This gives

$$k_{2,opt} = \frac{R_2}{2}\left[G_1\left(S^2 - 1\right) + 2S^2 R_2\right]. \tag{A15}$$

The corresponding optimal coupling coefficient $k_{1,opt}$ is obtained by replacing k_2 in Eq. (A13) with $k_{2,opt}$. The optimal relative bandwidth can be obtained by replacing k_2 in Eq. (A14) with $k_{2,opt}$. This gives

$$B_{dr,opt} = \frac{\sqrt{\left[G_1\left(S^2 - 1\right) + 2S^2 R_2\right]^2 - \left(2SR_2\right)^2}}{2S}. \tag{A16}$$

After the normalizations $\omega_{r1} = \omega_{r2} = \omega_c = 1$, $Z_0 = 1$, and $L_1 = L_2 = 1$, the relation between the resistive components (G_1 and R_2) and corresponding unloaded quality factors in Eqs. (A11) to (A16) is $G_1 = 1/Q_{01}$ and $R_2 = 1/Q_{02}$. By substituting these into Eq. (A16), it can be written

$$B_{dr,opt} = \sqrt{S^2 - 1}\sqrt{\frac{S^2 - 1}{4S^2} \cdot \frac{1}{Q_{01}^2} + \frac{1}{Q_{01}Q_{02}} + \frac{1}{Q_{02}^2}}. \tag{A17}$$

In the case of a lossless resonant matching circuit, i.e. $Q_{01} = \infty$, Eq. (A17) simplifies to

$$B_{dr,opt} = \frac{\sqrt{S^2 - 1}}{Q_{02}}. \tag{A18}$$

HELSINKI UNIVERSITY OF TECHNOLOGY RADIO LABORATORY REPORTS

S 238 Räisänen, A.V.
Opinnäytetyöt radiotekniikassa 1924-1999
Theses in Radio Engineering 1924-1999, July 1999

S 239 Sehm, T.
Development of Low-profile Radio Link Antennas for Millimeter Waves, February 2000

S 240 Vainikainen, P., Ollikainen, J., Kivekäs, O., Kelander, I.
Effect of Phone Chassis on Handset Antenna Performance, March 2000

S 241 Räisänen, A.V., Lindberg, S.
HUT Radio Laboratory Research and Education 1999, April 2000

S 242 Lundén, O-P.
Low Noise Amplifiers and Local Oscillators for Wireless Communications Receivers, April 2000

S 243 Nyfors, E.
Cylindrical Microwave Resonator Sensors for Measuring Materials under Flow, April 2000

S 244 Kivinen, J.
Development of Wideband Radio Channel Measurements and Modeling Techniques for Future Radio Systems, March 2001

S 245 Räisänen, A.V., Lindberg S.
HUT Radio Laboratory Research and Education 2000, March 2001

S 246 Ala-Laurinaho, J.
Numerical Studies on a Radio Frequency Hologram and its Use in Antenna Measurements, May 2001

S 247 Juntunen, J.
Selected Developments in Computational Electromagnetics for Radio Engineering, May 2001

S 248 Tretyakov, S.
Waveguide and Antenna Theory, July 2001

S 249 Kalliola, K., Sulonen, K., Laitinen, T., Kivekäs, O., Krogerus, J., Vainikainen, P.
Angular Power Distribution and Mean Effective Gain of Mobile Antenna in Different Propagation Environments, September 2001

S 250 Icheln, C.
Methods for measuring RF radiation properties of small antennas, November 2001

S 251 Kalliola, K.
Experimental analysis of multidimensional radio channels

ISBN 951-22-5891-9
ISSN 1456-3835